Microchim Acta (2011) 175:55–61
DOI 10.1007/s00604-011-0649-5

ORIGINAL PAPER

Synthesis of multi-branched gold nanoparticles by reduction of tetrachloroauric acid with Tris base, and their application to SERS and cellular imaging

Zhihui Luo · Tao Fu · Kun Chen · Heyou Han · Mingqiang Zou

Received: 26 February 2011 / Accepted: 24 June 2011 / Published online: 12 July 2011

Abstract We show that tris base (TB), a widely used buffer substance, can act as a reducing agent to synthesize multi-branched gold nanoparticles (mb-AuNPs) from tetrachloroauric acid in a one-step process. The method is simple, fast, and inexpensive and produces mb-AuNPs that are virtually monodisperse, have a size of about 90 nm and typically >6 branches. Their UV-vis absorption peaks can be fine-tuned from the visible to the near-infrared (NIR) region by controlling the concentration of TB. The mb-AuNPs represent an efficient substrate for surface-enhanced Raman scattering (SERS), with an enhancement factor of 1.2×10^5. They were applied as substrates for SERS-based imaging of kidney cells.

Keywords Multi-branched gold nanoparticles · Tris base · Synthesis · Surface-enhanced Raman scattering · Cell imaging

Introduction

Over the past decade, increasing interest and research investigations have been focused on gold nanostructures owing to their unique physicochemical properties and potential applications in catalysis [1, 2], biosensing [3–5] and SERS detection [6–8] etc. The unique physicochemical properties of gold nanostructures are greatly affected by their size, shape, and crystal structure, and therefore it is possible to tune the properties of gold nanostructures by tailoring the morphology of gold nanostructures [9]. These mb-AuNPs, as excellent SERS substrates, have higher SERS activity than the sphere-shaped gold nanoparticles (ss-AuNPs) because of the strong enhancement of the electromagnetic field at the tips of the NPs [8, 10, 11]. Many different shapes of AuNPs have been developed, including spheres, nanopeanuts, tetrapods, dendrite-like and flower-shaped NPs [12–15] etc. Conventionally, mb-AuNPs are successfully synthesized through seeding growth approaches with the help of some directing agents including the surfactant [16–18], electrochemical method [19, 20], hydrothermal method [21], vapor phase polymerization method [22] and seedless in situ growth method [10, 23]. However, only a few reports are available on facile synthesis of mb-AuNPs by seedless in situ growth with small biomolecules. In addition, other methods proved to be much more complicated, time-consuming and used intrinsically cytotoxic surfactants [24]. Recently, controlled synthesis of various shaped gold nanostructures with "clean", environmentally friendly or tractable surface is one of the new development trends in nanomaterials' biological applications [9, 25, 26]. It will be highly desirable to develop a simple, rapid and low-cost method for the synthesis of mb-AuNPs in aqueous solutions. Raj' group prepared flower-like Au NPs using a relatively "green" chemical, 2-[4-(2-hydroxyethyl)-1-piperazinyl] ethanesulfonic acid (HEPES), as both reducing and shape directing agents, and the obtained products showed excellent electrocatalytic activity toward the oxidation of

Electronic supplementary material The online version of this article (doi:10.1007/s00604-011-0649-5) contains supplementary material, which is available to authorized users.

Z. Luo · T. Fu · K. Chen · H. Han (✉)
State Key Laboratory of Agricultural Microbiology,
College of Science, Huazhong Agricultural University,
Wuhan 430070, People's Republic of China
e-mail: hyhan@mail.hzau.edu.cn

M. Zou (✉)
Chinese Academy of Inspection and Quarantine,
Beijing 100025, People's Republic of China
e-mail: mingqiangz@sina.com

methanol and the reduction of oxygen [27]. More recently, Xie et al. synthesized mb-AuNPs with a high yield and good monodispersity using HEPES, and proposed that piperazine in the HEPES molecule was responsible for forming highly branched Au nanocrystals [8, 28]. Nevertheless, it still remains a challenge to develop facile, low-cost and template-free methods for preparing anisotropy Au NPs.

Tris base (TB), as a common organic compound, has been extensively used as a component of pH buffer solutions and is usually employed to prepare an important organic intermediate, Schiff base. The TB molecule possesses three hydroxyl groups which can serve as the active group to reduce noble metal ions forming nanocrystals [29]. Here, we report a facile method for preparing high-quality mb-AuNPs using TB as the ideal reducing agent without any surfactant or seed. The effects of experimental variables on the morphology of the products were systematically investigated and the formation mechanism of mb-AuNPs is also discussed. As a SERS-active substrate, the mb-AuNPs showed high SERS activity and were successfully applied in cell imaging.

Experimental

Materials

Hydrochloroauric acid trihydrate, tris-base, ethylene diamine, glycerol, 2-Amino-2-methyl-1,3-propanediol, 1,3-Propanediol and ethanol were purchased from Shanghai Chemical Reagent Co. (Shanghai, China. http://sinoreagent.cn.alibaba.com). 4-mercaptobenzoic acid (4-MBA) was obtained from Tokyo Chemical Industry Co., Ltd. (Tokyo, Japan. http://www.tci-asiapacific.com). All other chemicals were of analytical grade. Cow kidney cell was provided by the College of Veterinary Medicine, Huazhong Agricultural University. All of the solutions were prepared with ultrapure water.

Synthesis of multi-branched gold nanoparticles

All glassware used in the preparation of mb-AuNPs were cleaned with freshly prepared aqua regia and rinsed thoroughly with ultrapure water. In a typical synthesis, 0.09 g TB was dissolved in 5 mL of ultrapure water, and 100 μL of 48 mmol·L^{-1} $HAuCl_4$ solution was added under magnetic stirring for 15 min, followed by adjusting the pH to 11 by dropwise addition of 1.0 mol·L^{-1} NaOH solution. Afterward, the reaction vessel was transferred to a water bath and maintained at 60 °C for 60 min. The solution color changed from light yellow to purple and finally blue-green. The products were purified for three times by centrifugation at 8000 rpm, and the resultant precipitates were re-dissolved in ultrapure water for further use.

Characterization

The UV-vis absorption spectra of mb-AuNPs were recorded on a Thermo Nicolet 300 spectrophotometer (Thermo Nicolet, US. http://www.thermoscientific.com). The morphologies of mb-AuNPs were obtained from a transmission electron microscope (TEM, Hitachi, Japan. http://www.hitachi-hitec.com) after placing a drop of the purified products onto a Cu grid. Scanning electron microscopy (SEM) images were preformed with an S-4800 (Hitachi, Japan. http://www.hitachi-hitec.com) operating at 5 KV. X-ray diffraction (XRD) analysis of mb-AuNPs was carried out with a Rigaku D/MAX-RB diffractometer (Rigaku, Japan, http://www.rigaku.com) with Cu Kα radiation (λ=0.15406 nm). FT-IR spectra were collected on a Nicolet Avatar-330 spectrometer (Thermo Nicolet, US. http://www.thermoscien9tific.com) with 4 cm^{-1} resolution using the KBr pellet technique. SERS were obtained using an Invia Raman spectrometer (Renishaw, UK. http://www.renishaw.com) equipped with a confocal microscope (Leica, German. http://www.leica-microsystems.com). The excitation source (He-Ne laser (633 nm)) was used in the experiment. For the measurement of enhancement factors (EF), a 20 × objective lens was used to focus a laser spot on a capillary tube with a power of approximately 20 mW. The Raman spectra were collected for 10 s exposure times, 2 accumulations in the range of 400–2000 cm^{-1}.

Results and discussion

Synthesis and characterization of multi-branched gold nanoparticles

In order to demonstrate the reducing ability of TB, UV-Vis absorption spectra were applied to investigate each of the resulting NPs during the experiments. As shown in Fig. 1, the $HAuCl_4$ solution has an intense absorption band at 292 nm due to the metal to ligand charge transfer band from the $AuCl_4$-complex [30, 31], and the colorless TB solution has no specific absorption band in the visible region (curve a, Fig. 1). When TB was added to the $HAuCl_4$ solution, the solution color faded. The appearance of a new absorption peak at 330 nm as seen in curve c in Fig. 1 might be explained by the formation of TB-Au complex. However, with the help of heating at 60 °C, the maximum surface plasmon absorbance peak of Au NPs was observed at 650 nm in the presence of TB (curve b, Fig. 1), while there was no obvious absorption peak after 500 nm without the addition of TB (curve d, Fig. 1). The result was consistent with the absorption features of mb-AuNPs prepared by other reported methods [8–10]. Moreover, the color change of the reaction solution partially confirmed this hypothesis. As indicated by the inset in Fig. 1, the aqueous gold chloride

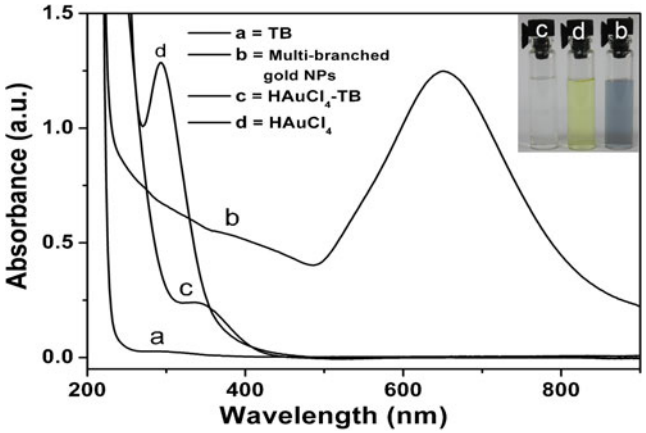

Fig. 1 UV-Vis absorption spectra of different precursor solutions and the mb-AuNPs. Curves a and d show the absorption spectra of TB (0.15 mol·L^{-1}) and $HAuCl_4$ solution (0.96 mmol·L^{-1}), respectively. Curve c and b show the absorption spectra of the mixture of $HAuCl_4$ solution with TB before and after heating. The inset shows three different color photographs: b, mb-AuNPs solution after 60 min of heating (pH=11); c, $HAuCl_4$ solution with TB before heating; d, $HAuCl_4$ solution

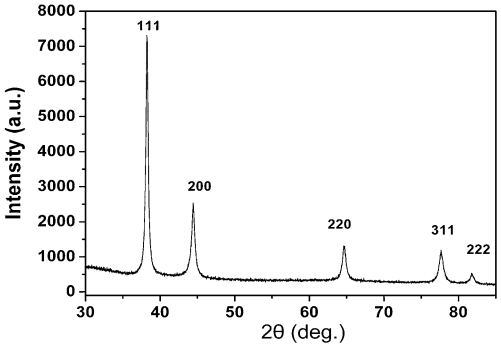

Fig. 3 The XRD pattern of the mb-AuNPs by the reduction of $AuCl_3^-$ ions (0.96 mmol·L^{-1}) in 0.45 mol·L^{-1} TB solution

solution turned gradually from light yellow at the very beginning to blue-green when reacted at 60 °C for 60 min. These results preliminarily inferred the formation of gold nanostructures from the reduction of $HAuCl_4$ by TB.

TEM and SEM were employed to confirm the morphology and structure of the metal nanostructures. As shown in Fig. 2, these mb-AuNPs are nearly monodisperse NPs with an average size of 90 nm, and most of them possess more than six branches. The roughened surface determined by the branches and the cavities of multi-branched NPs increases the particle total surface area which may provide many 'hot spots' due to localized electromagnetic field enhancement. Figure 3 displays the XRD pattern of the mb-AuNPs. Five peaks including 38.11°, 44.35°, 64.56°, 77.53°, 81.7°, could be respectively assigned to the reflections of (111), (200), (220), (311), and (222) faces from the centered cube structure of metallic gold. The result confirmed the crystallinity of the mb-AuNPs [32]. In addition, the intensity ratio (0.35) of the (200) diffraction peak to the (111) diffraction peak is lower than that of bulk material (≈0.53), indicating that the product is primarily dominated by (111) faces [33].

Effect of the pH of solution

It is worth pointing out that the pH of solution had great effects on the formation of gold nanostructures in this reaction system. To better understand the reducing capacity of TB, we varied the pH of $HAuCl_4$ solution containing 0.15 mol·L^{-1} TB from 3 to 11, as shown in Fig. S1 (Electronic Supplementary Material, ESM). When the pH values of $HAuCl_4$-TB solution were lower than 8, no gold nanostructures formed after 1 h or even more time. When the pH was adjusted to 9 and 10, the solution color turned to fuchsia and violet blue after 2 h of heating, corresponding to the absorption peaks at 596 and 608 nm, respectively, which indicated the formation of Au NPs. Nevertheless, at a pH of 11, the absorption of Au NPs was located at 652 nm after 60 min of reaction. The shorter growth time suggested that the reducing ability of TB might be improved in the presence of extra OH^- ions [31, 34, 35].

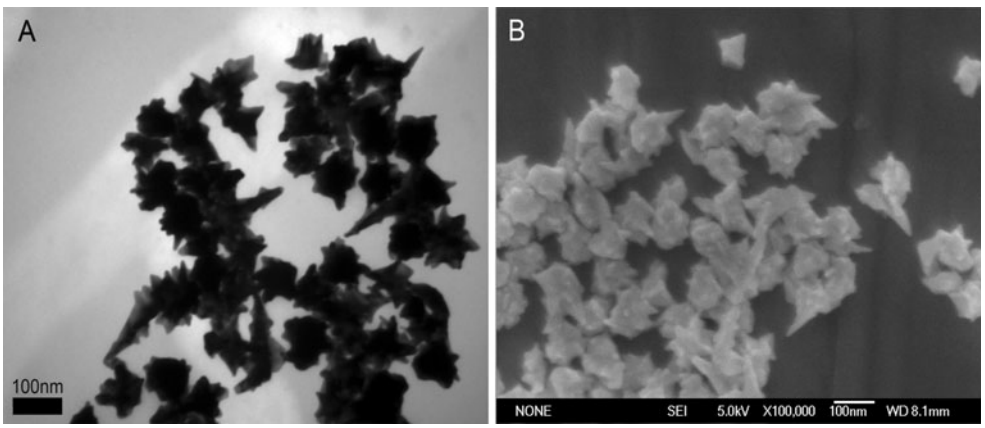

Fig. 2 TEM and SEM images of the mb-AuNPs by the reduction of $AuCl_3$ ions (0.96 mmol·L^{-1}) in 0.45 mol·L^{-1} TB solution

Effect of concentration of tris base

In the following experiments, it was found that the size and morphology of the NPs depend greatly on the concentration of TB. As shown in Fig. S2 (ESM), with the increase of TB concentration from 0.0017 to 0.45 mol·L^{-1}, the maximum absorption peak of the products shifted from 528 to 758 nm, which indicated that the Au NPs might gradually evolve from a sphere to a multi-branched shape [9]. Briefly, at low TB concentration (0.0017 mol·L^{-1}), the synthesized products exhibited spherical nanostructures, and their sizes varied within 30 nm (Fig. S2 A, ESM). When the TB concentration increased to 0.012 mol·L^{-1}, irregularly shaped NPs were observed (Fig. S2 B, ESM). With increasing TB concentration, the morphology of the NPs evolved from an irregular shape to a multi-branched shape, and eventually grew into long multi-branched nanostructures (Fig. S2 (C-E), ESM). Hence, we carefully chose the TB concentration in the synthetic process.

The formation mechanism of multi-branched gold nanoparticles

The formation of mb-AuNPs could be attributed to the direct reduction of $HAuCl_4$ by the TB molecule since there was no other reducing agent in the system. El-Sayed et al. [36] provided two reasonable explanations for the formation of faceted particles: (i) the growth rates vary at different planes of the particles; (ii) particle growth competes with the coordinating action of stabilizers. On the basis of these explanations, a possible growth mechanism of mb-AuNPs was proposed as shown in Fig. 4c. First, $HAuCl_4$ was reduced to a gold atom by TB in the solution at 60 °C, these gold atoms spontaneously coalesced to form Au clusters and then gradually grew into small Au NPs. Second, the small gold NPs further agglomerated into anisotropic gold nanostructures due to the reduced surface energy [8]. Finally, with the addition of increasing amounts of TB, the anisotropic feature of gold nanostructures grew further because the amino group of molecular TB was adsorbed onto the surface of NPs to form a covalent bond with gold [37]. In order to verify our hypothesis, TEM and IR spectra were carried out to characterize the products. As shown in Fig. 4b, the NPs evolved from a sphere shape to a thumb-like and further to a long branched shape with the reaction time. The IR curves of TB and the mb-AuNPs have some similarities, although some of the bands shift due to surfaced chemisorption, as revealed in Fig. 5, the characteristic absorption bands at 3340, 3290 and 3190 cm^{-1} are characteristics of the stretching of the N-H bond vibration modes, while the absorption band at 1630 and 1590 cm^{-1} are assigned to bending vibration of the N-H bond. In addition, the absorption bands around 2850 and 2920 cm^{-1} are assigned to symmetric stretching vibration and asymmetric stretching vibration of -CH_2 vibration modes. The absorption band at 1025 cm^{-1} is attributed to stretching vibration of the C-N bond, that at 1390 cm^{-1} is assigned to tertiary carbon stretching vibration modes [38, 39]. Mb-AuNPs was also investigated using a Raman spectrometer. As shown in Fig. S3 (ESM), the low frequency band at 287 cm^{-1} is assigned to stretching vibration of the Au-N bond [40], while the bands at 1020 cm^{-1} and 1068 cm^{-1} are attributed to stretching vibration of the C-N bond and twisting vibration of -NH_2 [41, 42]. Considering the IR spectra, the results indicated that TB molecules were adsorbed on the surface of the mb-AuNPs because of surfaced chemisorption with gold during the reaction.

To further confirm the speculation, five different reductants including 2-amino-2-methyl-1, 3-propanediol, glycerol, ethylene diamine, ethanol and 1, 3-propanediol, were used to synthesize gold nanostructures under the same conditions. The resulting products were characterized by TEM and UV-vis absorption spectra. As shown in Fig. S4 (ESM), mb-AuNPs were only observed in 2-amino-2-methyl-1, 3-propanediol solution (Fig. S4 A, ESM), whereas ss-AuNPs were formed in glycerol, 1, 3-propanediol and ethanol (Fig. S4 (B-D), ESM) solutions,

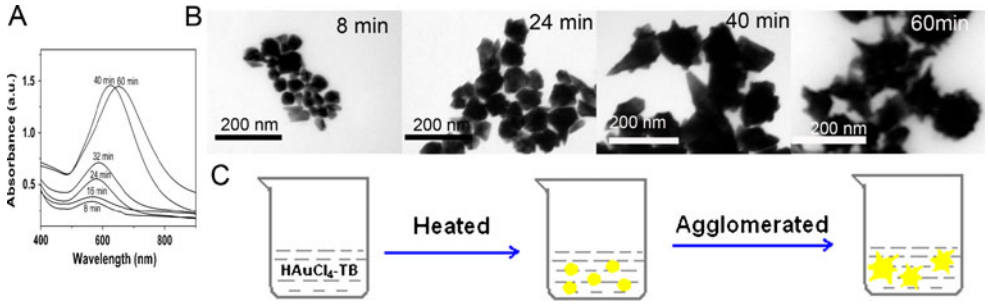

Fig. 4 **a** UV-Vis absorption spectra of Au NPs as a function of reaction time. The $HAuCl_4$ and TB concentrations were 0.96 m mol·L^{-1} and 0.15 mol·L^{-1}, respectively. **b** TEM images of the obtained products at 8, 24, 40, and 60 min during the reaction. **c** Schematic illustration of the main steps involved in the synthesis of the mb-AuNPs

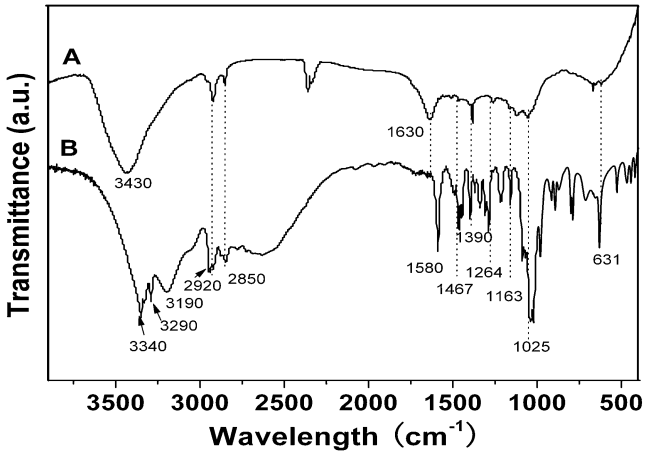

Fig. 5 IR spectra of the mb-AuNPs (**a**) and TB (**b**)

gold NPs could not be prepared in ethylene diamine solution. The surface plasmon absorbance band of Au NPs reduced by 2-amino-2-methyl-1, 3-propanediol was located at 578 nm, while the absorption peaks of the NPs reduced by other reductants occurred at 530 nm (Fig. S4 F, ESM). It is well known that these compounds bearing hydroxyl groups serve as weak reducing agents which have been widely used to reduce noble metal salts [29, 43]. Compared with the structure of these compounds (Fig. S4 E, ESM), it becomes clear that TB, 2-amino-2-methyl-1, 3-propanediol, glycerol, 1, 3-propanediol and ethanol all have a hydroxyl group except ethylene diamine, while TB and 2-amino-2-methyl-1, 3-propanediol possess one amino group. Thus ethylene diamine could not reduce $HAuCl_4$ to Au NPs due to the lack of hydroxyl groups. The amino group in TB and 2-amino-2-methyl-1, 3-propanediol was responsible for the adsorption of these molecules to the Au surface, which stabilized and directed the crystal growth. The amino group may be most accountable for the formation of mb-AuNPs, without which ss-AuNPs would form exclusively.

Multi-branched gold nanoparticles as active SERS substrates for cell imaging

Previous theoretical and experimental investigations had revealed that mb-AuNPs exhibited intense local electromagnetic field enhancement, which could serve as SERS substrates for biological sensing. The Raman spectra of ethanol, pure MBA in ethanol, MBA adsorbed on the mb-AuNPs and 50 nm ss-AuNPs are shown in Fig. S5 (ESM). The Raman vibrations at 520, 1076, 1173, 1394, and 1586 cm^{-1} can be observed in (Fig. S5 D curve, ESM). Among them, the prominent SERS bands at 1076 and 1586 cm^{-1} are attributed to the ν_{12} and ν_{8a} aromatic ring vibrations, respectively [44, 45]. In curve A of the Fig. S5 (ESM), the characteristic peak at 880 cm^{-1} is assigned to in-plane stretching vibration of C-C-O, the bands at 1052, 1097 cm^{-1} are assigned to out-plane stretching vibration of C-C-O, the band at 1454 cm^{-1} is attributed to asymmetric stretching vibration of $–CH_3$ [46]. These Raman bands of ethanol are not interfered with by Raman bands of MBA at 1586 cm^{-1}. In order to estimate their SERS activity, the equation $(EF=(I_{SERS}/I_{Raman})/(C_{SERS}/C_{Raman}))$ was used to calculate the SERS activity of mb-AuNPs and ss-AuNPs [23]. Where I_{SERS} and I_{Raman} are the intensity of the ν_{8a} (1586 cm^{-1}) in the SERS and normal Raman spectra of the solution, respectively, C_{SERS} and C_{Raman} are the concentrations of MBA in the SERS sample (1.0×10^{-6} mol·L^{-1}) and pure MBA solution (0.1 mol·L^{-1}). The calculated EF values are 1.2×10^5 and 5.3×10^4 for the mb-AuNPs and ss-AuNPs, respectively. As predicted, the mb-AuNPs exhibited a stronger SERS signal than the ss-AuNPs. The results were

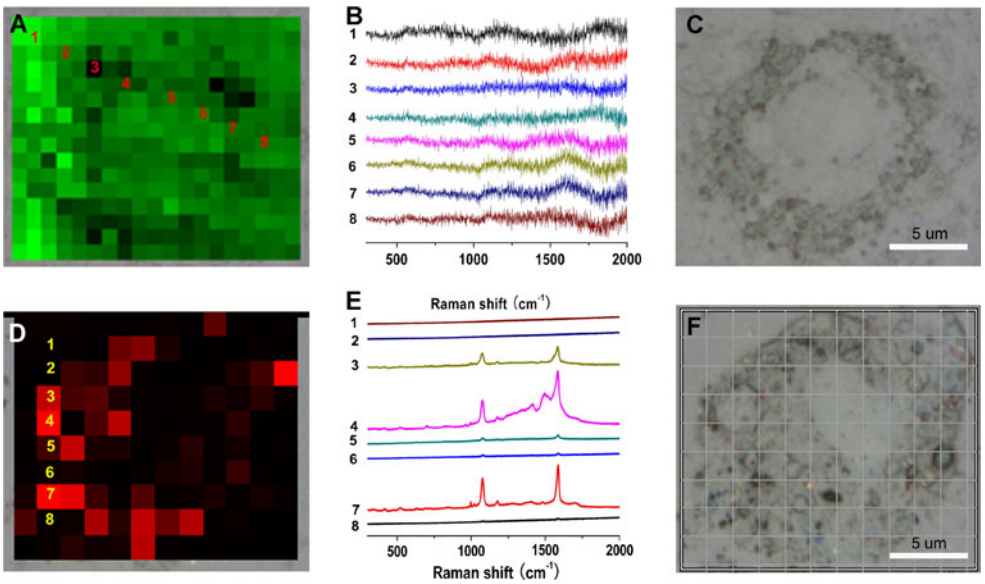

Fig. 6 Optical microscopy of a single milk cow cell before (**c**) and after uptake of the mb-AuNPs nanoprobes (**f**). Raman mapping images of this cell before (**a**) and after (**d**) uptake of the the mb-AuNPs nanoprobes. SERS spectra of this cell before (**b**) and after (**e**) uptake of the mb-AuNPs nanoprobes

very similar to those reported in the literature [8]. Based on their good biocompatibility and low cyctotoxicity, Au NPs exhibited a large potential in biological sensing. We investigated the SERS behavior of mb-AuNPs with cow kidney cells as model. In the experiment, the mb-AuNPs were first capped by poly(vinyl pyrrolidone) (PVP) after labelling with MBA. Here, PVP functions as a capping reagent to prevent MBA from leaking from the surface of the mb-AuNPs. It also serves as a solubilizer to increase the biocompatibility of the nanoprobes [47]. Then, 400 μL of the mb-AuNPs nanoprobes solution was incubated with cow kidney cell, followed by fixing the cells on the glass slides by formaldehyde after 5 h, and finally washing three times with phosphate buffered saline (pH=7.2). Another group was used as a control group in the absence of mb-AuNPs nanoprobes. The microscopy image of a single cow kidney cell under Raman mapping in Fig. 6 clearly indicates that the mb-AuNPs nanoprobes were successfully taken up. The corresponding SERS of the cells are consistent with their images. At different positions of the cells, SERS of nanoprobes could be detected (Fig. 6e), while the control showed no SERS signal (Fig. 6b). It is indicated that the mb-AuNPs nanoprobes had great biocompatibility. The conservation of the SERS effect in cells suggested that the mb-AuNPs nanoprobes could be suitable for in vitro detection and have potential for in vivo applications.

Conclusions

In summary, we have developed a facile, low-cost and eco-friendly method to synthesize mb-AuNPs employing TB molecules as reductant and directing reagent in the absence of surfactants and seeds. The morphology and size of the gold nanostructures were well controlled by varying the $HAuCl_4$/TB molar ratio. The mb-AuNPs possessed a tunable absorption property ranging from the visible to the NIR spectrum and high SERS activity. The amino groups of TB molecules plausibly dominated the growth of the mb-AuNPs. More importantly, this nanomaterial exhibited favorable biocompatibility for in vivo cell imaging. Our preliminary results illustrated that this material can potentially be applied to biomolecular detection and photothermal therapy.

Acknowledgement The authors gratefully acknowledge the support for this research by the National Natural Science Foundation of China (20975042), the Program for Academic Pacesetter of Wuhan (200851430484), Nature Science Foundation key project from Hubei Province of China (2008CDA080), International Science and Technology cooperation and Exchange Foundation (2008DFA40270), the Fundamental Research Funds for the Central Universities of China (2009JC005) and Genetically Modified Major Projects (2009ZX08012-015B).

References

1. Kundu S, Lau S, Liang H (2009) Shape-controlled catalysis by cetyltrimethylammonium bromide terminated gold nanospheres, nanorods, and nanoprisms. J Phys Chem C 113:5150
2. Mohanty A, Garg N, Jin R (2010) A universal approach to the synthesis of noble metal nanodendrites and their catalytic properties. Angew Chem Int Ed 49:4962
3. Larsson EM, Alegret J, Kall M, Sutherland DS (2007) Sensing characteristics of NIR localized surface plasmon resonances in gold nanorings for application as ultrasensitive biosensors. Nano Lett 7:1256
4. Luo Z, Chen K, Lu D, Han H, Zou M (2010) Synthesis of p-aminothiophenol-embedded gold/silver core-shell nanostructures as novel sers tags for biosensing applications. Microchimica Acta doi:10.1007/s00604-010-0537-4
5. Shao M, Lu L, Wang H, Luo S, Ma D (2009) Microfabrication of a new sensor based on silver and silicon nanomaterials, and its application to the enrichment and detection of bovine serum albumin via surface-enhanced Raman scattering. Microchimica Acta 164:157
6. Rodríguez-Lorenzo L, Álvarez-Puebla RA, García J, de Abajo F, Liz-Marzán LM (2010) Surface enhanced Raman scattering using star-shaped gold colloidal nanoparticles. J Phys Chem C 114:7336
7. Joseph D, Geckeler KE (2009) Surfactant-directed multiple anisotropic gold nanostructures: synthesis and surface-enhanced Raman scattering. Langmuir 25:13224
8. Xie J, Zhang Q, Lee JY, Wang DIC (2008) The synthesis of SERS-active gold nanoflower tags for in vivo applications. ACS Nano 2:2473
9. Wang Z, Zhang J, Ekman JM, Kenis PJA, Lu Y (2010) DNA-mediated control of metal nanoparticle shape: one-pot synthesis and cellular uptake of highly stable and functional gold nanoflowers. Nano Lett 10:1886
10. Bakr OM, Wunsch BH, Stellacci F (2006) High-yield synthesis of multi-branched urchin-like gold nanoparticles. Chem Mater 18:3297
11. Giannini V, Rodríguez-Oliveros R, Sánchez-Gil JA (2010) Surface plasmon resonances of metallic nanostars/nanoflowers for surface-enhanced Raman scattering. Plasmonics 5:99
12. Lokesh K, Narayanan V, Sampath S (2009) Phthalocyanine macrocycle as stabilizer for gold and silver nanoparticles. Microchimica Acta 167:97
13. Divsar F, Nomani A, Chaloosi M, Haririan I (2009) Synthesis and characterization of gold nanocomposites with modified and intact polyamidoamine dendrimers. Microchimica Acta 165:421
14. Chen S, Wang ZL, Ballato J, Foulger SH, Carroll DL (2003) Monopod, bipod, tripod, and tetrapod gold nanocrystals. J Am Chem Soc 125:16186
15. Xie W, Su L, Donfack P, Shen A, Zhou X, Sackmann M, Materny A, Hu J (2009) Synthesis of gold nanopeanuts by citrate reduction of gold chloride on gold-silver core-shell nanoparticles. Chem Commun 35:5263
16. Sau TK, Murphy CJ (2004) Room temperature, high-yield synthesis of multiple shapes of gold nanoparticles in aqueous solution. J Am Chem Soc 126:8648
17. Nehl CL, Liao H, Hafner JH (2006) Optical properties of star-shaped gold nanoparticles. Nano Lett 6:683
18. Ahmed W, Kooij ES, Silfhout A, Poelsema B (2010) Controlling the morphology of multi-branched gold nanoparticles. Nanotechnology 21:125605
19. Xu X, Jia J, Yang X, Dong S (2010) A templateless, surfactantless, simple electrochemical route to a dendritic gold nanostructure and its application to oxygen reduction. Langmuir 26:7627
20. Han X, Wang D, Huang J, Liu D, You T (2011) Ultrafast growth of dendritic gold nanostructures and their applications in methanol

electro-oxidation and surface-enhanced Raman scattering. J Colloid Interface Sci 354:577
21. Tang XL, Jiang P, Ge GL, Tsuji M, Xie SS, Guo YJ (2008) Poly(n-vinyl-2-pyrrolidone) (PVP)-capped dendritic gold nanoparticles by a one-step hydrothermal route and their high SERS effect. Langmuir 24:1763
22. Tamil Selvan S (1998) Novel nanostructures of gold-polypyrrole composites. Chem Commun 3:351
23. Jeong G, Lee Y, Kim M, Han S (2009) High-yield synthesis of multi-branched gold nanoparticles and their surface-enhanced Raman scattering properties. J Colloid Interface Sci 329:97
24. Yuan H, Ma W, Chen C, Zhao J, Liu J, Zhu H, Gao X (2007) Shape and SPR evolution of thorny gold nanoparticles promoted by silver ions. Chem Mater 19:1592
25. Wang T, Hu X, Dong S (2006) Surfactantless synthesis of multiple shapes of gold nanostructures and their shape-dependent sers spectroscopy. J Phys Chem B 110:16930
26. Li L, Weng J (2010) Enzymatic synthesis of gold nanoflowers with trypsin. Nanotechnology 21:305603
27. Jena BK, Raj CR (2007) Synthesis of flower-like gold nanoparticles and their electrocatalytic activity towards the oxidation of methanol and the reduction of oxygen. Langmuir 23:4064
28. Xie J, Lee JY, Wang DIC (2007) Seedless, surfactantless, high-yield synthesis of branched gold nanocrystals in hepes buffer solution. Chem Mater 19:2823
29. Au L, Lim B, Colletti P, Jun Y, Xia Y (2009) Synthesis of gold microplates using bovine serum albumin as a reductant and a stabilizer. Chem-Asian J 5:123
30. Mason WR, Gray HB (1968) Electronic structures and spectra of square-planar gold(III) complexes. Inorg Chem 7:55
31. Kundu S, Wang K, Liang H (2009) Size-selective synthesis and catalytic application of polyelectrolyte encapsulated gold nanoparticles using microwave irradiation. J Phys Chem C 113:5157
32. Maye MM, Zheng W, Leibowitz FL, Ly NK, Zhong CJ (1999) Heating-induced evolution of thiolate-encapsulated gold nanoparticles: a strategy for size and shape manipulations. Langmuir 16:490
33. Kim F, Connor S, Song H, Kuykendall T, Yang P (2004) Platonic gold nanocrystals. Angew Chem Int Ed 43:3673
34. Caruso RA, Ashokkumar M, Grieser F (2002) Sonochemical formation of gold solutions. Langmuir 18:7831
35. Kundu S, Pal A, Ghosh SK, Nath S, Panigrahi S, Praharaj S, Pal T (2004) A new route to obtain shape-controlled gold nanoparticles from Au(III)-β-diketonates. Inorg Chem 43:5489
36. Petroski JM, Wang ZL, Green TC, El-Sayed MA (1998) Kinetically controlled growth and shape formation mechanism of platinum nanoparticles. J Phys Chem B 102:3316
37. Prasad BLV, Stoeva SI, Sorensen CM, Klabunde KJ (2003) Digestive-ripening agents for gold nanoparticles: alternatives to thiols. Chem Mater 15:935–942
38. Zhang J, Misra RDK (2007) Magnetic drug-targeting carrier encapsulated with thermosensitive smart polymer: core-shell nanoparticle carrier and drug release response. Acta Biomaterialia 3(6):838–850
39. Hou X, Zhang X, Fang Y, Chen S, Li N, Zhou Q (2010)1-hexadecylamine as both reducing agent and stabilizer to synthesize Au and Ag nanoparticles and their SERS application. J Nano Res doi:10.1007/s11051-010-9945-y
40. Faggiani R, Howard-Lock HE, Lock CJL, Turner MA (1987) The reaction of chloro(triphenylphosphine)gold(I) with 1-methylthymine. Can J Chem 65:1568
41. Nakamoto K (1986) Infrared and Raman spectra of inorganic and coordination compounds, 4th edn. John Wiley & Sons
42. Lan GX, Shi XP, Hu SF, Wang HF, Lu MK, Zhang PL (1989) Raman spectra of trihydroxymethylaminomethane phosphate crystal. Guang Pu Xue Yu Guang Pu Fen Xi of China 10:12
43. Li W, Guo Y, Zhang P (2010) SERS-active silver nanoparticles prepared by a simple and green method. J Phys Chem C 114:6413
44. Michota A, Bukowska J (2003) Surface-enhanced Raman scattering (SERS) of 4-mercaptobenzoic acid on silver and gold substrates. J Raman Spectrosc 34:21
45. Orendorff CJ, Gole A, Sau TK, Murphy CJ (2005) Surface-enhanced Raman spectroscopy of self-assembled monolayers: sandwich architecture and nanoparticle shape dependence. Anal Chem 77:3261
46. Ye Q, Xu Q, Yu Y, Qu R, Fang Z (2009) Rapid and quantitative detection of ethanol proportion in ethanol-gasoline mixtures by Raman spectroscopy. Optics Communications 282:3785–3788
47. Tan XB, Yang J, Song CY, Zhang RH, Cui YP (2009) Polyvinylpyrrolidone (PVP) coated silver aggregates for high performance surface-enhanced Raman scattering in living cells. Nanotechnology 20:445102